Variability in surface reflectance of the Greenland ice sheet (1982-2005) using satellite remote sensing

A Senior Honor's Thesis

Presented in Fulfillment of the Requirements for graduation with distinction in Atmospheric Science in the undergraduate colleges of the Ohio State University

By

Bruce A. Veenhuis

The Ohio State University
June 2006

Project Advisor: Dr. Jason Box, Department of Geography, Byrd Polar Research Center

Abstract

Data from space born sensors, the Advanced Very High Resolution Radiometer (AVHRR) and the Moderate Resolution Imaging Spectroradiometer (MODIS) are used to investigate albedo trends over the entire Greenland ice sheet for the period 1982-2005. Data from the two sensors is merged in order to performing an extended trend analysis, as the current publicly available AVHRR data only covers the period from 1982-1999. Satellite derived albedo measurements are compared with *in-situ* automatic weather station albedo values in order to assess sensor biases and inter-calibrate the datasets. Comparing AVHRR and MODIS with *in-situ* observations yields mean biases of -0.032 and -0.050 and root mean square errors of 0.093 and 0.075, respectively. Dataset inter-calibration is attempted using the mean biases as offsets and by calibrating each albedo image to the dry snow constant. Dataset in-homogeneity issues are not entirely resolved; therefore trend analysis is performed separately for each data record. AVHRR registers statistically significant mean albedo reductions as large as 0.08 over the southern ice sheet and ice sheet periphery. Albedo remained unchanged over the interior dry-snow region. MODIS period data reveal additional reductions, with albedo decreasing more than 0.08 along the ice sheet margins during the early melt season (i.e., April 1- June 31). Investigation of albedo-temperature correlation yields statistically significant values at the 99% level as great as -0.8 along ice sheet margins, where melting strongly influences albedo.

Glossary

Albedo - Percent of total received shortwave radiation (0.4-1.7 μm) reflected by a surface.

AVHRR - Advanced Very High Resolution Radiometer

AWS - Automatic Weather Station

EOS - Earth Observing System

GC-Net - Greenland Climate Network

IDEA - Improved Direct Estimate Algorithm

LWIR - LongWave InfraRed (8-15 μm)

MODIS - Moderate Resolution Imaging Spectroradiometer

MS2GT - MODIS Swath to Grid Toolbox

NAO - North Atlantic Oscillation

NIR - Near InfraRed (0.8-1.4 μm)

Polar MM5 - Polar Mesoscale Model version 5

R - Pearson's correlation coefficient

RMSE - Root Mean Square Error

SWIR - ShortWave InfraRed (1.4-3 μm)

TOA radiance - Top Of the Atmosphere radiance

1 Introduction

Surface albedo is critical in determining surface radiation budgets and melt rates, as it governs the magnitude of absorbed solar energy (e.g. Ohmura, 1999). Fresh snow, having a high albedo, reflects up to 84% of incident solar radiation (Warren, 1984). During melt, the presence of dust and liquid water can reduce snow albedo by more than a factor of 2, amplifying melt. Due to this positive feedback, amplified climate changes are expected in the polar-regions. Accurate albedo assimilation is thus vital for climate and mass balance models attempting to predict climate change (Stroeve et al., 2005).

The Greenland ice sheet, unlike the Antarctic, undergoes substantial summer melting with fresh water discharge comprising half the annual mass loss (Zwally and Giovinnetto, 2000). The mass balances of ice sheets is imprecisely known (e.g. van der Veen, 2001); however, studies suggest the Greenland ice sheet mass balance may be slightly negative (Box et al., 2004, 2006). The Greenland ice sheet is believed to have played and important role in past global sea-level fluctuations (Cuffey and Marshall, 2000) and is predicted to contribute more to future sea-level rises than Antarctica (Gregory and Oerlemans, 1998).

The topography of the Greenland ice sheet rises from less than 1000 m near the ice sheet margin to over 3000 m at the ice sheet summit. Before the onset of melt, the Greenland ice sheet has a high uniform albedo of approximately 0.84 at all elevations (Warren, 1984) (**Figure 1.1**). As the melt season progresses, melt ponds form at lower elevations, darkening the surface (Gruell and Oerlemans, 2002). Albedo decreases to a minimum in late August at the end of the melt-season (Luthje et al., 2006). The average

melt-season duration varies from a minimum of 0 days in the interior to over 100 days along the southwestern ice sheet margin (Box et al., 2004).

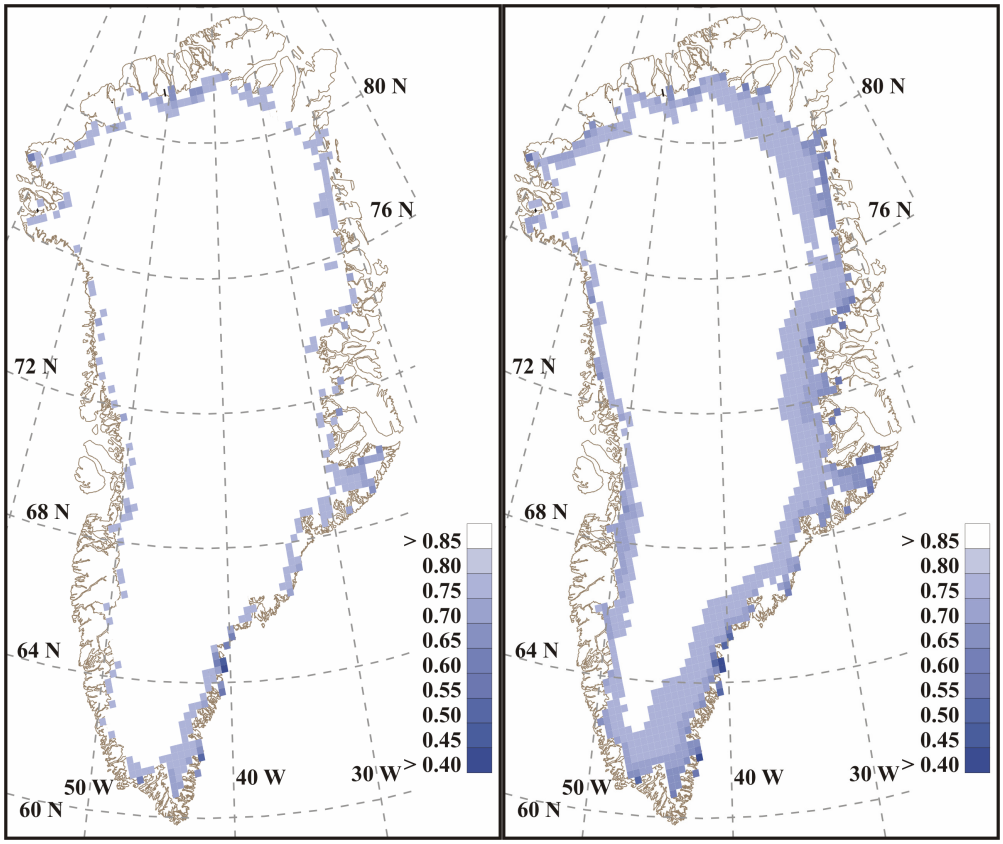

Figure 1.1 Monthly mean satellite-derived albedo. Left (April - Pre-melt), Right (August - Late-melt)

Recent studies suggest significant changes are occurring in the Greenland climate regime. Box et al. (2006) used calibrated Polar MM5 data to model Greenland ice sheet climate for the period 1988-2004. The study found positive temperature trends, with melt-season duration increasing a maximum of 1.7 weeks per year in response to widespread warming. Greatest warming trends were situated along the ice sheet periphery. Investigation of Greenland coastal stations reveals variable temperature trends (Box, 2002); however, a general 1-4° C warming occurred over the 1991-2000 period.

Other studies have used satellite passive microwave remote sensing to monitor Greenland ice sheet melt extent. For example, Abdalati and Steffen (2001) analyzed passive microwave data for the period 1979-1999 finding a 1% year^{-1} positive melt extent trend for the entire ice sheet. This study concluded that the observed trend was governed primarily by increased melt in the western ablation region, driven by a 1 °C surface air temperature increase. Warming temperatures increase Greenland ice sheet freshwater discharge (Box et al. 2006) and potentially alter oceanic circulations (Clark et al., 2002).

Space-borne sensors on polar orbiting satellites provide broad spatial surface albedo records over the Arctic (Stroeve, 2001). For this study, albedo data from the Advanced Very High Resolution Radiometer (AVHRR) and the Moderate Resolution Imaging Spectroradiometer (MODIS) are analyzed to reveal trends over the 1982-2005 period. Previous studies that have used AVHRR satellite-derived albedo to analyze trends over the Arctic include; Arctic sea-ice albedo (Laine, 2004) and Greenland ice sheet albedo (Stroeve, 2001). No previous study has attempted to combine AVHHR and MODIS albedo data to perform an extended trend analysis over the Greenland ice sheet. The merger of the datasets is done in order to extend the satellite-derived albedo to 2005. In addition the MODIS instrument has superior specifications to AVHRR making albedo derivation potentially more accurate. The evaluation of sensor error and bias is critical for merging the datasets. The Greenland Climate Network (GC-Net) (Steffen et al., 1996) provides *in-situ* albedo observations for this evaluation.

2 Data

a. Satellite Albedo Data

Satellite Sensors

AVHRR has been flown onboard a series of NOAA polar orbiting satellites since 1978, measuring reflected solar radiation in five spectral bands with a maximum resolution of 1km (**Table 2.1**). This study uses 24km resolution albedo data from the Extended AVHRR Polar Pathfinder (APP-x) dataset (Key, 2002). The APPx dataset is comprised of data from AVHRR sensors flown on the NOAA satellites NOAA-7,-9,-11, and -14. As this dataset contains albedo from multiple sensors, calibrations have been performed to remove sensor biases (Key, 2001). AVHRR geo-location errors are typically 2-3 km, however the error can be as a large as 10-12 km, creating a potential error source.

Table 2.1 AVHRR specifications. Bands 1 and 2 are used to derive albedo.

	AVHRR Specifications	
Band	Wavelength (μm)	Spectral Region
1	0.58-0.68	Visible
2	0.725-1.0	NIR
3	3.55-3.93	SWIR
4	10.3-11.3	LWIR
5	14.4-12.4	LWIR

MODIS on the NASA Terra and Aqua satellites measures energy in 36 spectral bands, with 250m resolution in bands 1 and 2. Launched in 2000, onboard Terra, MODIS provides improved spectral resolution over AVHRR (Stroeve et al., 2005). Daily 1km resolution MOD02 and MOD03 granules, which contain 5 minute data swaths, were gathered from the NASA Earth Observing System (EOS) data gateway for

the Terra afternoon pass (~15:00z). All available melt-season data (April 1- Sept. 20) are obtained spanning a 6-year period, that is, 2000-2005. The MOD02 granules contain top of the atmosphere (TOA) radiances for the 36 spectral bands while MOD03 files provide geo-location data. MODIS TOA radiance from bands 1, 2, 3, 4, 5, 6, and 7 (**Table 2.2**) are utilized in the derivation of broadband albedo. The narrow to broadband conversion is described in the **Methods** section **3.a.**

Table 2.2 MODIS instrument specifications for bands used in this study.

MODIS Specifications		
Band	Wavelength (nm)	Spectral Region
1	620 - 670	Red
2	841 - 876	NIR
3	459 - 479	Blue
4	545 - 565	Green
5	1230 - 1250	SWIR
6	1628 - 1652	SWIR
7	2105 - 2155	SWIR

Data Coverage

Satellite observations provide daily albedo data spanning the 1982-2005 period. Figure 2.1 shows the frequency of daily albedo data used in this study. Occasional data gaps exist during the MODIS data record. Investigation into the causes of MODIS data gaps was inconclusive, with few publications addressing the issue. Most of these data gaps are small (i.e. less than 10 days); however, it is noteworthy that data are missing for the entire month of April 2005 and for parts of June 2003 and 2001. It may be important to consider these interruptions when analyzing the results. The AVHRR data record

appears to have complete seasonal coverage with no extended data disruptions (Key, 2001).

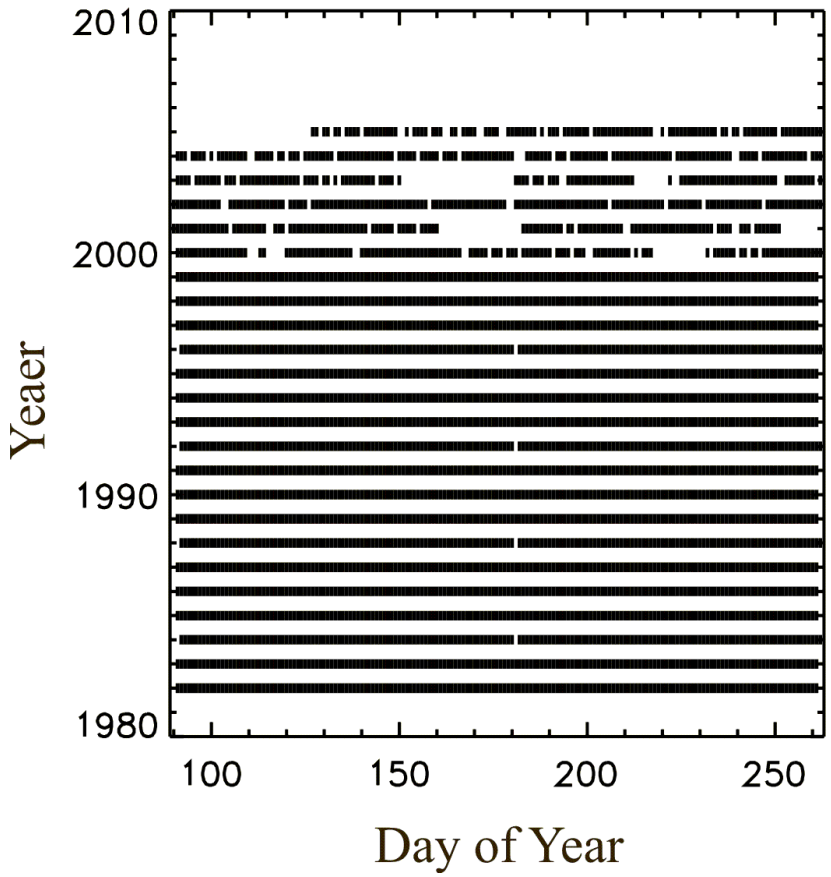

Figure 2.1 Daily albedo data coverage for the period 1982-2005.

b. Greenland Climate Network

The Greenland Climate Network (GC-Net) is an array of 27 automatic weather stations (AWS) positioned in different glaciological zones over the Greenland ice sheet. Operational since a single installation at Swiss Camp in 1991, the network now provides extensive *in-situ* measurements of temperature, wind profiles, accumulation, humidity, and radiation balances (Steffen and Box, 1996). The validation procedure employs

albedo observations from 9 automatic weather station sites, spanning a broad range of surface conditions and melt duration. GC-Net AWS incident and reflected shortwave irradiance is measured at 15s intervals by LI-COR 200-SZ Silicon Photodiodes, and is averaged to produce hourly radiation fluxes (Steffen and Box, 2001). Daily mean albedo is calculated by integrating hourly radiance fluxes to obtain daily downward and upward shortwave irradiance totals (**Formula 2.1**). Calculating albedo from daily irradiance minimizes measurement errors due to solar zenith angles near 90° and instrument leveling errors (van den Broeke et al., 2004).

$$\alpha_I = \sum S\uparrow / S\downarrow$$

Formula 2.1 Calculation of "Integrated albedo" (α_I) where S↑ is the upward shortwave radiation flux and S↓ is the downward shortwave radiation flux.

d. Polar MM5 Data

Polar MM5 2 m surface air temperature data are available for the period 1991-2002. These data were produced as part of an ongoing effort to model the Arctic land ice surface mass budgets (Bromwich et al., 2005), (Box et al., 2004, 2006). The model was run over 3 nested domains with spatial resolutions of 72, 24, and 8 km respectively. Each domain used 28 vertical layers. A series of 30 hour forecasts were produced with output every 6 hours. Data from domain 2 (24 km), which covers Greenland, are used in this study. The temperature data have been calibrated using GC-Net AWS observations to remove a 1 °C warm bias (Box et al., 2004, 2006). An albedo-temperature correlation analysis is made using Polar MM5 data. Another sensitivity study explores increased melt potential using monthly mean Polar MM5 downward shortwave irradiance data.

3 Methods

a. Data Processing

The APP-x dataset provides AVHRR albedo measurements and does not require additional processing. To derive AVHRR surface albedo, top of the atmosphere (TOA) reflectance is calculated for the visible and near infrared channels (i.e., channels 1 and 2). An atmospheric correction is then applied, and solar and viewing angle corrections are performed to derive surface reflectance for bands 1 and 2. This narrow-band reflectance is converted to broadband albedo using **Formula 3.1**. Additional AVHRR APPx processing details can be found in Key, (2001).

$$\alpha = 0.0034 + 0.34\alpha_1 + 0.57\alpha_2$$

Formula 3.1 Narrow-band to broadband conversion for AVHRR sensor. Where α_1 and α_2 are narrow-band albedo for bands 1 and 2 (Key, 2001).

MODIS data require several processing steps to obtain surface albedo. First, the necessary data granules are obtained from the NASA Earth Observing System (EOS) data gateway. Two or three granules per day are required to provide complete Greenland ice sheet coverage, as each granule contains a five minute data swath with a spatial dimension of 2330x2000 km. The MODIS Swath to Grid Toolbox (MS2GT) (Haran, 2001) was run to create daily composite TOA radiance images from individual MODIS granules and interpolate the data to 24 km and 1.25 km resolution grids. The 24 km data are used for albedo trend analysis while the 1.25 km data are used to assess sensor bias in comparison with ground observations.

The Improved Direct Estimate Algorithm (IDEA) (Liang et al., 2005) calculates daily surface albedo from composite TOA radiance images. The IDEA is designed

specifically for snow and ice albedo retrieval and was found to produce an absolute error of 0.03 over the Greenland ice sheet (Liang et al., 2005). The algorithm provides a computationally efficient method to retrieve surface albedo from satellite-observed TOA radiances. Unlike other albedo algorithms, the IDEA avoids the need for detailed atmospheric corrections, instead relying on TOA radiances measured directly by the satellite instrument. Liang et al. (2005) describe the creation of the algorithm as a two step process. To develop IDEA extensive radiation transfer simulations were conducted using a radiation transfer model. During the simulations, aerosol optical depth, snow grain size, snow liquid water content, and solar and viewing angles were varied to simulate TOA radiances under a variety of atmospheric, surface, and viewing conditions. After creating this TOA radiance database, linear regression was used to derive albedo prediction formulas for various viewing and solar zenith angles. The algorithm is written in the Interactive Data Language (IDL) and relies on lookup tables generated by the radiation transfer simulations. To implement the algorithm, the user supplies the MODIS TOA radiances in bands 1, 2, 3, 4, 5, 6, and 7 as well as the solar zenith and viewing angle geometries. The algorithm predicts the most probable surface broadband albedo based on these parameters (Liang, et al., 2005).

NASA has developed a 16 day albedo product (Schaaf et al., 2002) validated over the Greenland ice sheet by Stroeve et al., (2005). The product was found to contain a mean bias of -0.05 relative to *in-situ* observations. In hopes of improving accuracy and to increase temporal resolution, daily albedo is derived using the IDEA.

b. Cloud Detection

Accurate cloud detection over snow and ice surfaces remains a source of uncertainty (e.g. Stroeve, 2001). Both snow and clouds tend to reflect highly in the visible portion of the electromagnetic spectrum. Over cold surfaces, such as the Greenland ice sheet, the snow surface and clouds may have approximately the same temperature, leading to similar infrared radiances. **Figure 3.1**, produced from a 1.25 km MODIS image, shows the radiation spectra for snow and cloud filled pixels. The greatest reflectance difference between snow and clouds occurs in MODIS band 6, corresponding to the near infrared portion of the spectrum (~1.6μm). Based on this information cloud detection is performed using a band 6 reflectance threshold of 0.15. Pixels with band 6 reflectance greater than 0.15 are classified as cloudy and assigned a flag value to later exclude them from albedo retrieval. A more advanced cloud clearing algorithm using brightness temperature thresholds (Trepte et al., 2001), was explored, but the algorithm did not significantly outperform a simple single channel threshold approach.

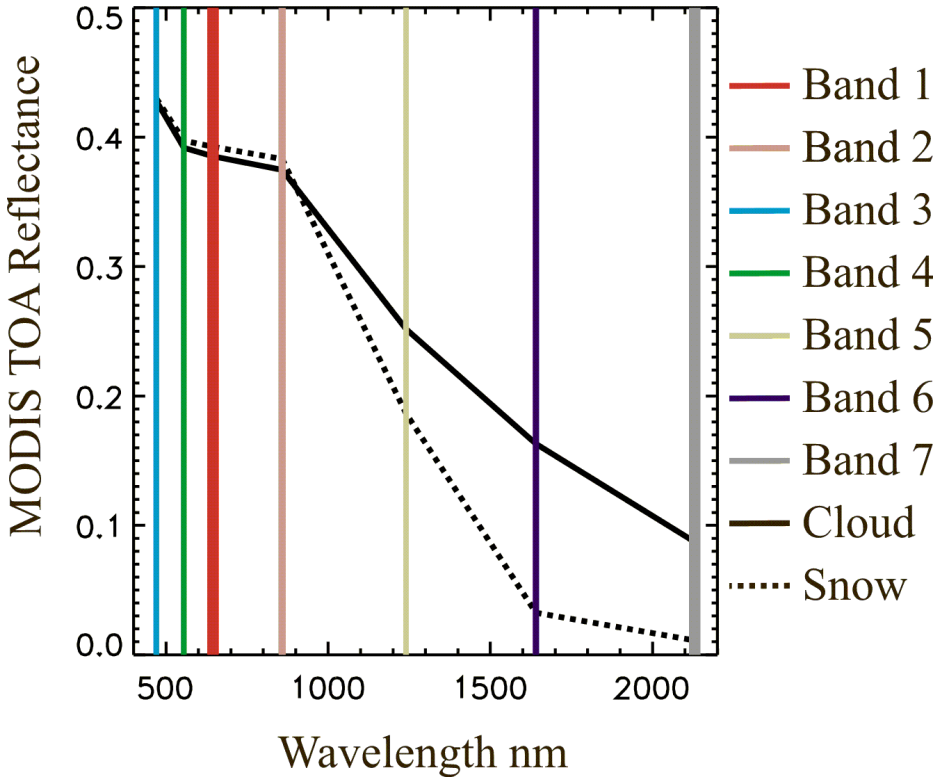

Figure 3.1 Reflectance spectra for clouds (solid line) and dry snow (dotted line). Vertical lines mark MODIS bands used in this study. Line width indicates band width.

c. Satellite-derived Albedo Validation and Dataset Inter-calibration

Several methods are used in an attempt to quantify sensor bias and inter-calibrate the datasets. The first method involves comparing satellite derived-albedo with albedo measured by GC-Net automatic weather stations (AWS). *In-situ* albedo data from Swiss Camp, NASA-U, Humboldt, Summit, DYE-2, JAR1, Saddle, NGRIP, and JAR2 are used for this comparison. JAR1 and JAR2 are located at elevations where seasonal melting and albedo fluctuations are largest. DYE-2 and Saddle exhibit some melting, but less than at the JAR sites. Swiss Camp corresponds to the so-called 'equilibrium line altitude', where annual mass loss is balanced by annual mass gain (i.e., net ablation ~0). Summit, NASA-U, NGRIP, and Humboldt are located in the so-called 'dry snow zone' and exhibit virtually no melting, with albedo remaining approximately constant at 0.84.

The varying melt climatologies of these automatic weather stations facilitate investigation of sensor bias under a variety of surface conditions.

24 km daily AVHRR albedo is compared with daily-integrated clear sky *in-situ* albedo for the year 1999. MODIS albedo validation is performed using 1.25 km IDEA data from the year 2001. MODIS cloud clearing was accomplished by visually inspecting each 1.25 km image using image texture variations to determine whether or not each automatic weather station location was cloud-covered. Satellite mean bias and root mean square error are calculated at each station for each year of operation and linear regression performed to measure the Pearson's correlation coefficient (R). In addition mean bias and root mean squared error (RMSE) are determined for the sensors using data from the 9 selected GC-Net AWS sites. The GC-Net LI-COR radiometers and IDEA are reported to have albedo measurement accuracies of 0.03 (Steffen and Box, 1996). Thus, any satellite-derived bias exceeding 0.03 is considered to be 'significant'.

Another method explored for removing satellite-derived albedo bias involves calibrating seasonal mean albedo images to match an assumed dry snow albedo (Warren, 1984). The melt season is divided into two parts, that is: early to mid melt (April 1 – June 30) and mid to late melt (July 1 – Sept. 20). Mean albedo is then calculated for each season for all years. The grid cell corresponding to Summit is selected to serve as a control. Seasonal mean albedo at Summit is subtracted from the dry snow albedo constant (0.84) (Konzelmann and Ohmura, 1995) to derive a calibration offset. The entire albedo image is then adjusted using this calibration offset. The premise for this calibration technique relies on the assumptions that sensor bias is constant for all albedo values and that the mean dry snow region albedo is 0.84.

d. Trend Analysis

Mean albedo is calculated for the first and last halves of the melt season using daily albedo files. Trends are measured at each data point as a linear regression slope coefficient over each time period. The linear trend is multiplied by the number of years to define the albedo 'change'. A two-sided Student's T-test is used to identify statistically significance trends at the 90%, 95%, and 99% confidence levels.

e. Albedo-Temperature Correlation Analysis

The half melt-season albedo images were used to investigate albedo-temperature correlation, melt sensitivity, and melt extent changes. The correlation between seasonal albedo and Polar MM5 2 m surface air temperature is calculated for each grid cell. Melt change induced by albedo change is explored using albedo trend data and Polar MM5 mean shortwave radiation fluxes. Melt extent changes are determined from the change in ice sheet area where significant melting is expected. Grid cells with mean albedo less than 0.7 (i.e., melting snow albedo) are defined as experiencing significant melt.

4 Results and Discussion

a. Satellite Comparison

Both AVHRR and MODIS surface albedo exhibited lower values than measured by GC-Net AWS. The bias is consistent between the satellite sensors. MODIS albedo data exhibit less random error than the AVHRR albedo but have a larger mean bias. Mean AVHRR and MODIS biases are -0.032 and -0.050 with RMSE values of 0.093 and 0.075 respectively (**Table 4.1**). This study suggests AVHRR and MODIS albedo measurements contain significant negative measurement biases that exceed GC-Net AWS albedo measurement error (that is 0.03). AVHRR bias results from the study agree with those from an earlier assessment by Stroeve et al. (2001). MODIS exhibits a more negative bias in this study than found by Liang et al., (2005). The discrepancy may be attributed to the use of the retrieval algorithm at solar zenith angles, up to 75°. Liang et al., (2005) cites that retrieval uncertainty increases with solar zenith angle; however a more conservative threshold (i.e. 60°) prevents complete Greenland ice sheet coverage. Accurate solar zenith and instrument viewing angle corrections are vital for satellite albedo measurements and remain an important source of uncertainty (Stroeve, 2001).

Table 4.1 Comparison of satellite-derived albedo with *in-situ* albedo. Biases are measured as *in-situ* observations minus satellite-derived observations.

	AVHRR (1999)			MODIS (2001)		
Station	Bias	RMS	N. Obs.	Bias	RMS	N. Obs.
Swiss Camp	-0.006	0.006	95	-0.035	0.039	13
NASA-U	-	-	0	-0.041	0.046	22
Humboldt	-	-	0	-0.067	0.071	24
Summit	0.003	0.027	10	-0.037	0.047	24
DYE-2	-0.017	0.017	48	-0.045	0.049	10
JAR1	0.004	0.004	67	-0.185	0.185	14
Saddle	-0.029	0.029	39	-0.046	0.056	16
NGRIP	-0.047	0.047	38	0.002	0.025	3
JAR2	0.09	0.093	89	0.007	0.039	20
All Stations	-0.032	0.093	386	-0.05	0.075	146

Scatterplots of satellite-derived albedo versus observed albedo at Swiss Camp, Summit, JAR1, JAR2 for AVHRR and MODIS are shown in **Figures 4.1** and **4.2**. AVHRR produces accurate albedo measurements for Swiss Camp and Summit with mean biases of -0.006 and 0.003, respectively. At JAR1 and JAR2, AVHRR albedo retrieval appears less accurate. Surface melt intensity most likely causes sensor performance variations. At JAR1 and JAR2, significant seasonal melting leads to melt lake formation and exposure of bare ice. Due to surface in-homogeneity, a point measurement may not represent the overall surface conditions measured by the 24 km grid cell. At Summit, there is little melting, while Swiss Camp experiences less intense melting. More homogenous surface conditions at Swiss Camp and Summit may explain the seemingly more accurate AVHRR albedo data.

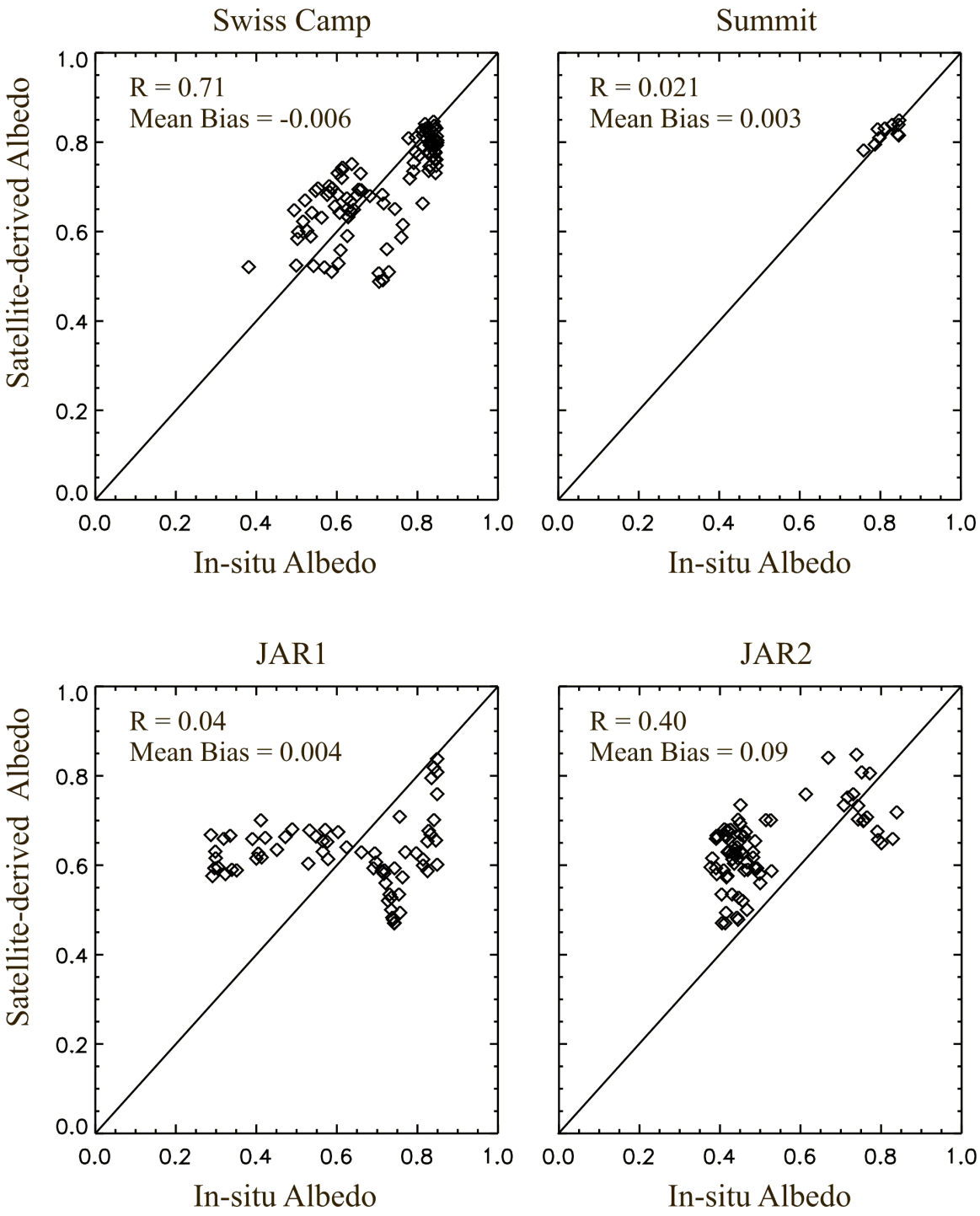

Figure 4.1 AVHRR satellite-derived albedo versus *in-situ* observations for 1999.

The MODIS albedo validation is conducted using 1.25 km resolution data. Scatterplots for Swiss Camp, Summit, JAR1, and JAR2 are shown in **Figure 4.2**. The MODIS data exhibit less RMS error than AVHRR. For instance, at Swiss Camp the correlation between *in-situ* and satellite derived-observations is high (R = 0.98) for MODIS. AVHRR correlation at Swiss Camp is lower (R = 0.71). MODIS also appears to better resolve surface in-homogeneity at JAR1 and JAR2 with correlations of 0.96 at both sites. A large MODIS bias (-0.185) is evident at JAR1 that is probably related to either surface in-homogeneity, GC-Net measurement error, or both. The *in-situ* radiometer may be viewing a bright snow patch in an area dominated by darker melt lakes and puddles. **Figure 4.3** shows the JAR1 AWS and its surroundings after complete loss of winter snow accumulation. Note the high spatial variability in surface albedo.

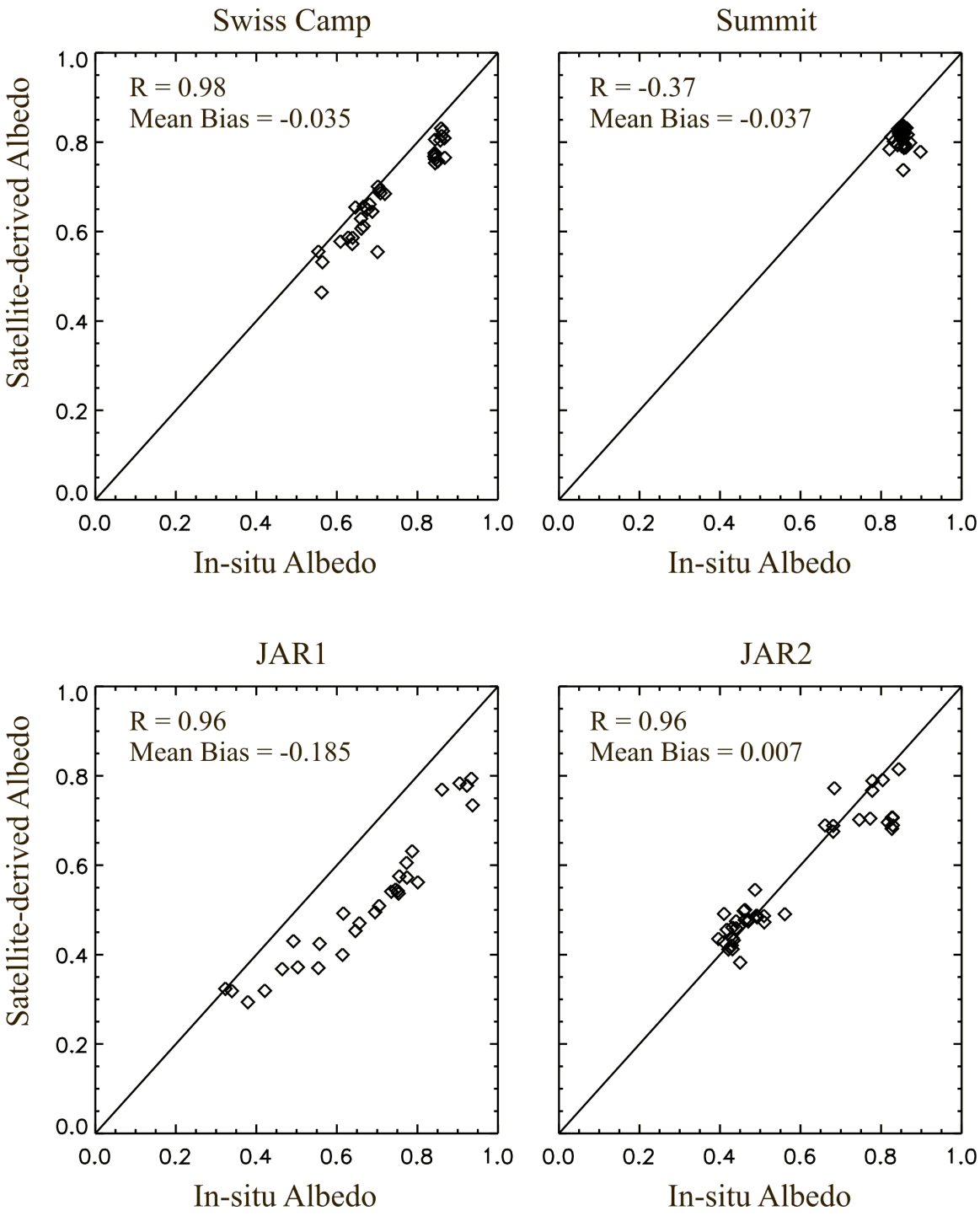

Figure 4.2 MODIS satellite-derived albedo versus *in-situ* albedo for 2001.

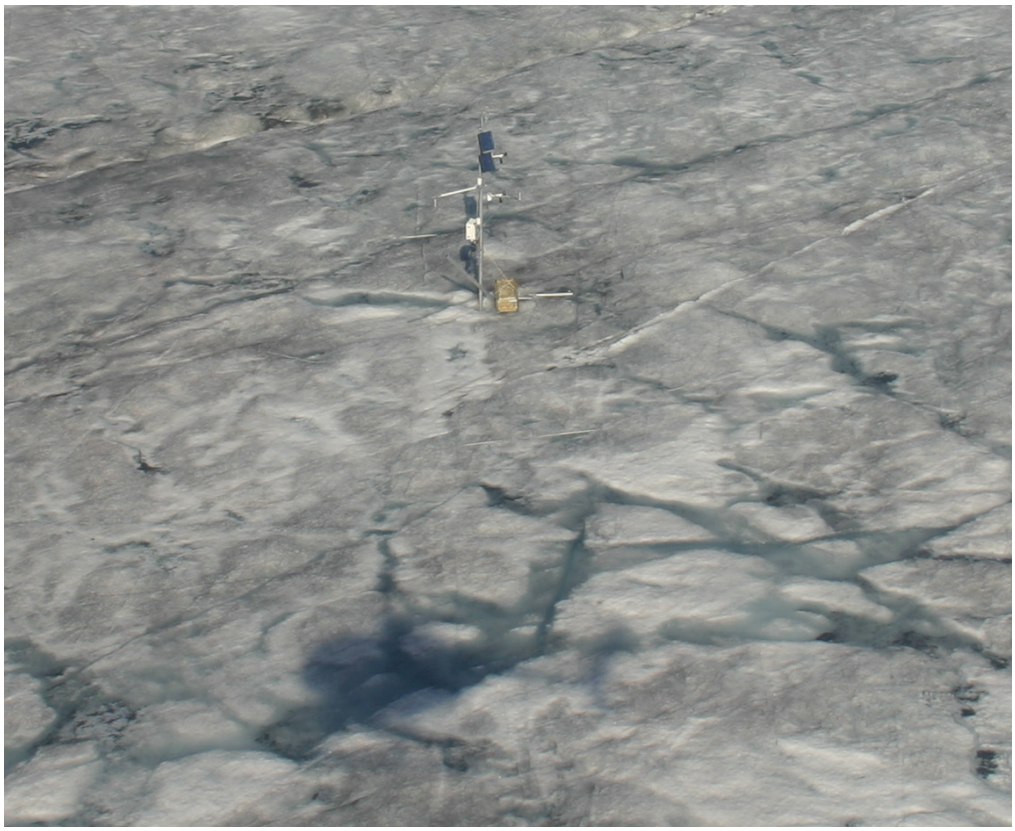

Figure 4.3 August 2005 aerial photo of JAR1 and its surroundings, photo by J. Box

The difference between dry snow zone albedo and the dry snow constant (i.e., 0.84) was explored using half melt mean albedo files. **Figure 4.4** presents the time series of calibration offsets derived for the early to mid and mid to late melt seasons. The offsets appear to fluctuate randomly over time. As the AVHRR record contains data from multiple sensors, the study suggests that the calibration by Key (2001) was successful in removing sensor biases. No bias trend is apparent during the AVHRR data period.

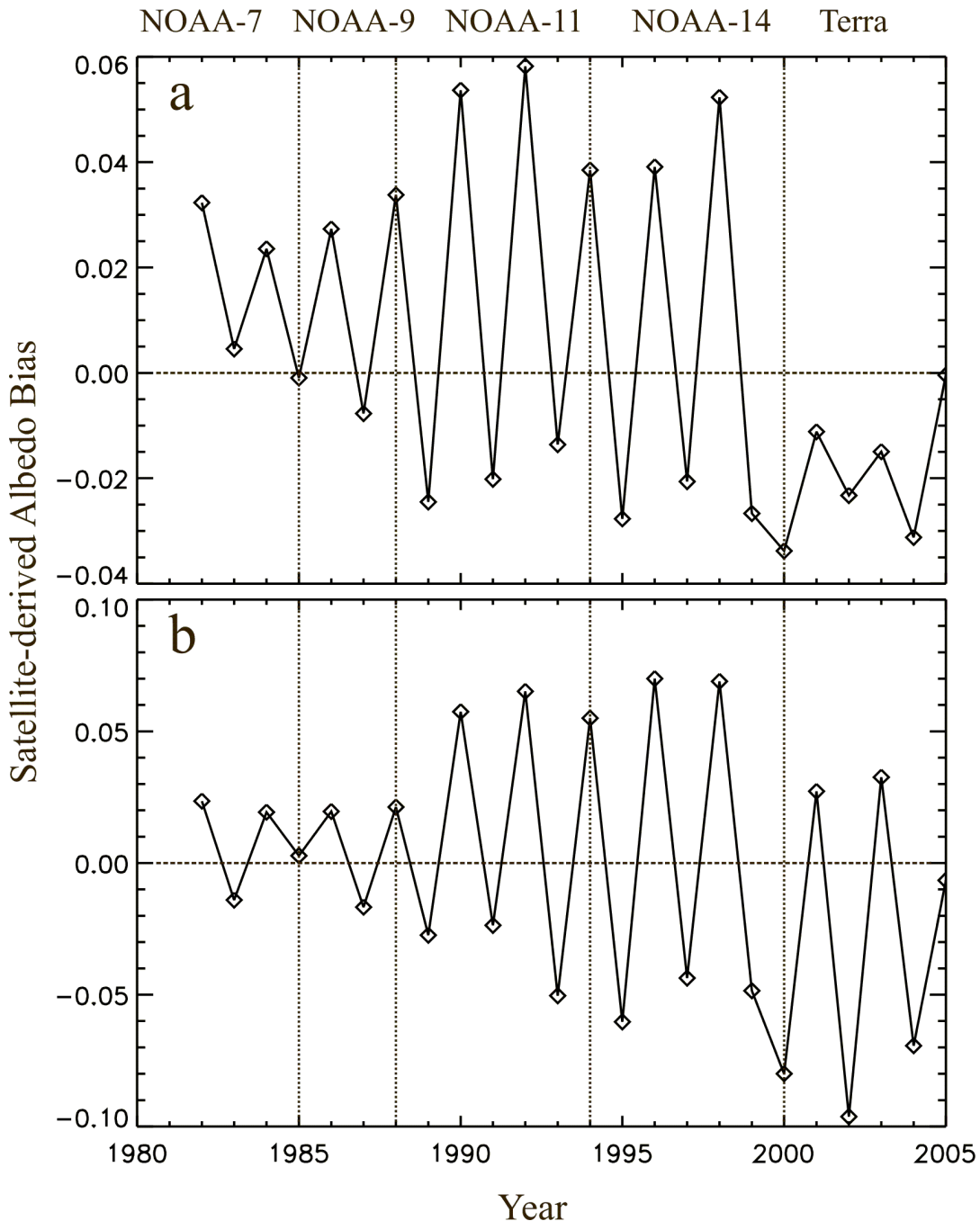

Figure 4.4 Time series of dry snow calibration offsets. Vertical lines differentiate between satellite missions. a.) Early to mid melt. b.) Mid to late melt.

b. AVHRR-MODIS Inter-Calibration

Inter-calibration of the data sets is attempted using the mean biases as offset corrections; however, sensor measurement differences are not fully resolved using this method. Calibrating each image to the dry snow constant is thus attempted to reduce temporal in-homogeneity. With both calibration methods, inherent sensor biases appear to mask underlying albedo trends. AVHRR-MODIS inter-calibration can not be reliably performed using only correction offsets, therefore trends are analyzed separately for each satellite data period. For analysis purposes sensor mean biases found by comparison with GC-Net AWS are removed.

c. Trend Analysis

Widespread seasonal mean albedo reductions, in some areas in excess of 0.08, are evident over the southern ice sheet and ice sheet periphery (**Figures 4.5** and **4.6**). Trends are only slightly negative or essentially zero over the interior dry snow zone. Small positive trends are confined to near-coastal locations in southwest and eastern Greenland. Both AVHRR and MODIS albedo trends are consistent in both melt-season periods.

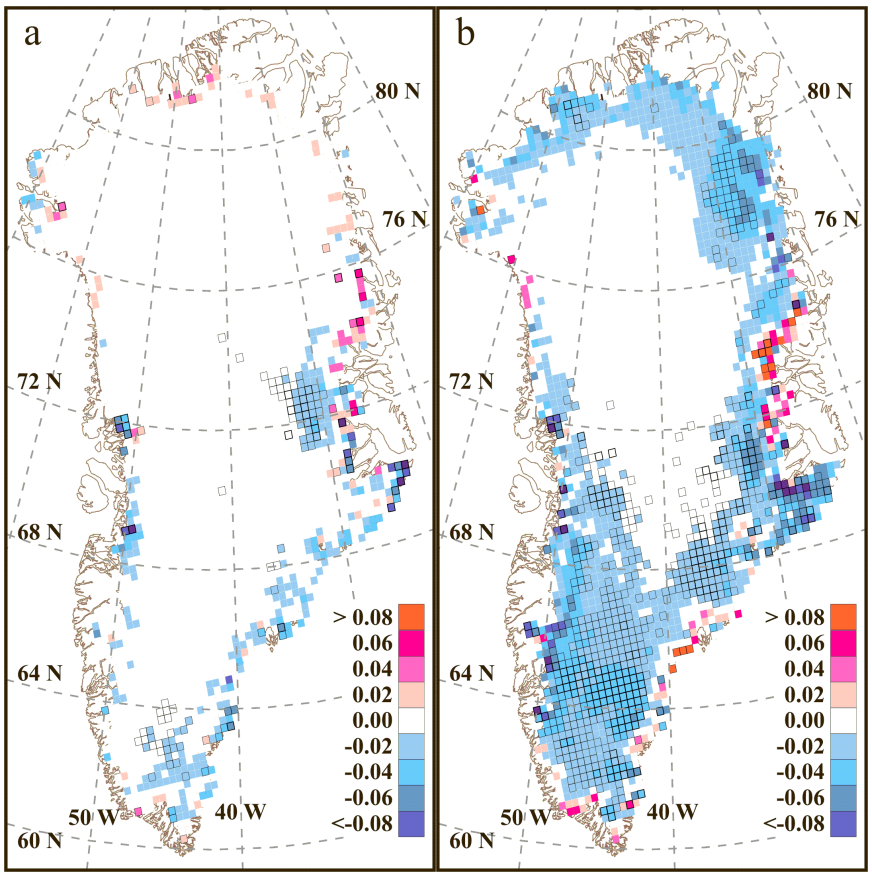

Figure 4.5 Mean seasonal albedo change for AVHRR data record, 1982-1999. Boxes indicate statistical significance at 90% (light grey), 95% (grey) and 99% (black). a.) Early to mid melt, b.) Mid to late melt.

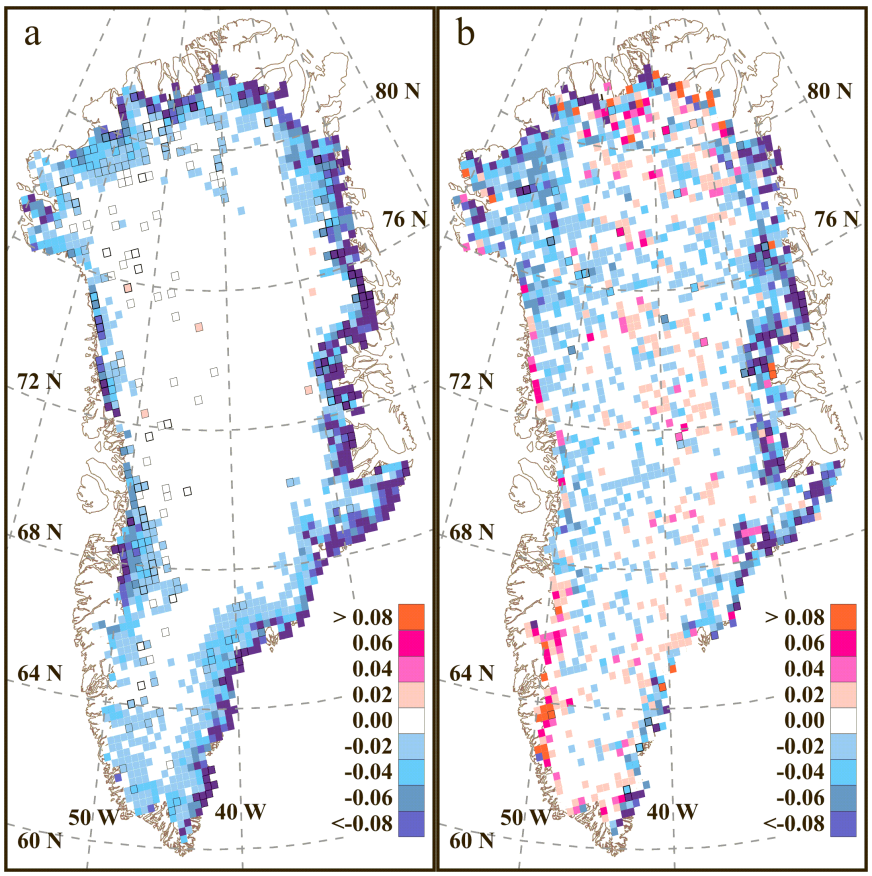

Figure 4.6 Mean seasonal albedo change for the MODIS data record, 2000-2005. Boxes indicate statistical significance at 90% (light grey), 95% (grey) and 99% (black). a.) Early to mid melt, b.) Mid to late melt.

Statistically significant trends at or above the 90%, 95%, and 99% confidence level found for AVHHR and MODIS using a two sided Student's T-test. Statistically significant trends at or above 90% percent confidence are widespread over the lower ice sheet elevations during the mid to late melt season for the AVHRR record.. Trends with statistical significance greater than 95% and 99% are confined mainly to western coastal regions for both AVHRR and MODIS periods. The relatively short MODIS record, that is, 6 years, and annual albedo variability may restrict the presence of statistically significant trends, as the Student's T-test is dependent on residual error and sample size.

The early to mid melt MODIS record contains a negative albedo trend extending along the entire eastern ice sheet periphery. However, this pattern is not statistically significant at the 90% threshold according to the Student's T-test. Polar MM5 2 m surface air temperatures for 1991-2002 do not display a spatially similar warming trend for the early to mid melt period. Warming after 2002 may be responsible for this trend and would not be present in the Polar MM5 data. Investigation of eastern Greenland coastal temperature records for the period 2000-2005 would facilitate trend assessment.

Trend analysis albedo reductions of 0.08 are considered to be 'significant' even if not passing T-Test thresholds because albedo changes are more than twice the data uncertainty, assumed to be 0.03. Using these criteria, significant negative albedo trends exist for both the AVHRR and MODIS data records.

Temperature, snow grain size and the presence of impurities are the primary factors that alter snow albedo (Warren, 1984). Positive temperature trends would generate negative albedo trends due to accelerated snow metamorphism, specifically, grain growth caused by increases in temperature and melt frequency (Warren, 1984). Snow grain growth reduces snow reflectivity, with larger grain sizes decreasing surface albedo (Bohren and Barkstorm, 1974). Specifically near infrared reflectance experiences the greatest albedo reduction.

West Greenland temperatures are somewhat controlled by large-scale atmospheric circulation via the so-called 'North Atlantic Oscillation' (NAO) (Box, 2002). A positive NAO index indicates anomalously low pressure south of Greenland and visa versa. Stroeve (2001) found a significant anti-correlation between Greenland ice sheet albedo and the NAO index. During a positive NAO phase, enhanced warm advection across the

southern ice sheet produces above normal temperature, increasing melt and lowering albedo. The impact of temperature on albedo is further explored in the following albedo-temperature correlation analysis.

The presence of impurities such as soil dust, volcanic ash, and black carbon lowers snow albedo (Warren, 1984). Black carbon, produced by fossil fuel combustion, has the largest impact on reflectivity properties, with an effect 200 times greater than volcanic dust (Wiscombe and Warren, 1980). The concentration and distribution of black carbon within the snow pack determine the magnitude of albedo change, with near-surface concentrations causing greater albedo reductions (Hansen et al., 2003). During melt black carbon may concentrate on the surface, amplifying albedo change (Grenfell et al., 2002). A black carbon concentration of 5-50 ppb may reduce snow albedo by 0.0-0.04 (Clark and Noone, 1985). A study conducted by Clarke and Noone (1985) found black carbon concentrations between 2-9 ppb in Greenland snow pits, suggesting albedo reductions of 0.005- 0.013 for new snow.

d. Albedo-Temperature Correlation Analysis

Albedo and temperature are correlated via the temperature-albedo feedback (Holland et al., 1997). The degree of albedo-temperature correlation depends partially on the seasonal albedo and temperature variations. **Figure 4.7** demonstrate the albedo-temperature co-variability. The strongest correlations ($R < -0.8$) occur at the lower elevations near the ice sheet margin, corresponding to the greatest melt, warmest temperatures, and largest seasonal albedo fluctuations. Correlations with statistical significance above 95% are widespread around the western and southern Greenland ice

sheet during the early melt season. Over the dry snow zone, the correlation diminishes, owing to little melt or temperature-driven snow grain metamorphosis.

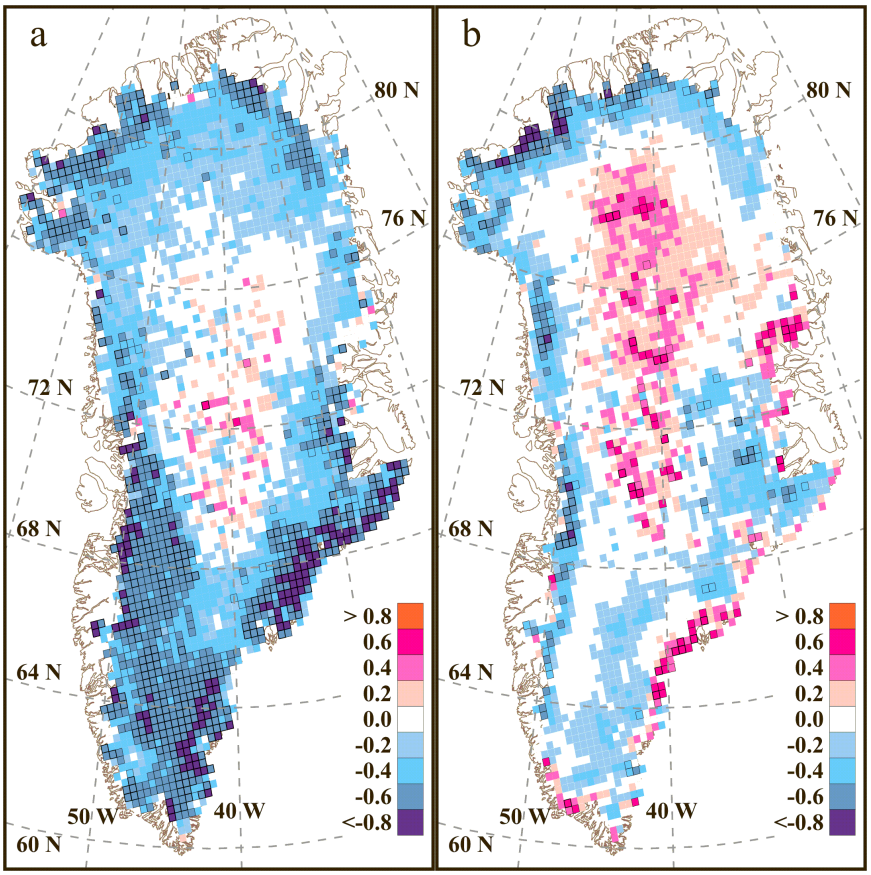

Figure 4.7 Correlation between albedo and temperature for the period 1991-2002. Boxes indicate statistical significance at 90% (light grey), 95% (grey) and 99% (black). a.) Early to mid melt, b.) Mid to late melt.

The temperature-albedo correlations are explored at GC-Net AWS (**Figure 4.8**). Linear regression is used to create albedo prediction formulas based on mean temperature. The correlation appears stronger for the early to mid melt season compared to the mid to late melt season. At JAR1, early melt season correlation is -0.884, but is reduced to 0.311 during the mid to late melt season. The progressive decrease in temperature-albedo correlation may be due to decreased variability of late melt season

temperature. Once the snow surface begins to melt, latent energy sinks (i.e. melt and evaporation) dominate the energy budget. A net air to surface energy transfer, maintains a negative sensible heat flux thus dampening surface air temperature variability. Adiabtic compression of down sloping katabatic winds and the downward shortwave radiation flux help maintain a negative sensible heat flux by renewing the sensible energy content of the air. Physical considerations that energy sinks dampen surface air temperature variability are substantiated by surface energy budget data collected by the JAR1 AWS (J. Box, personal communication, May 2006).

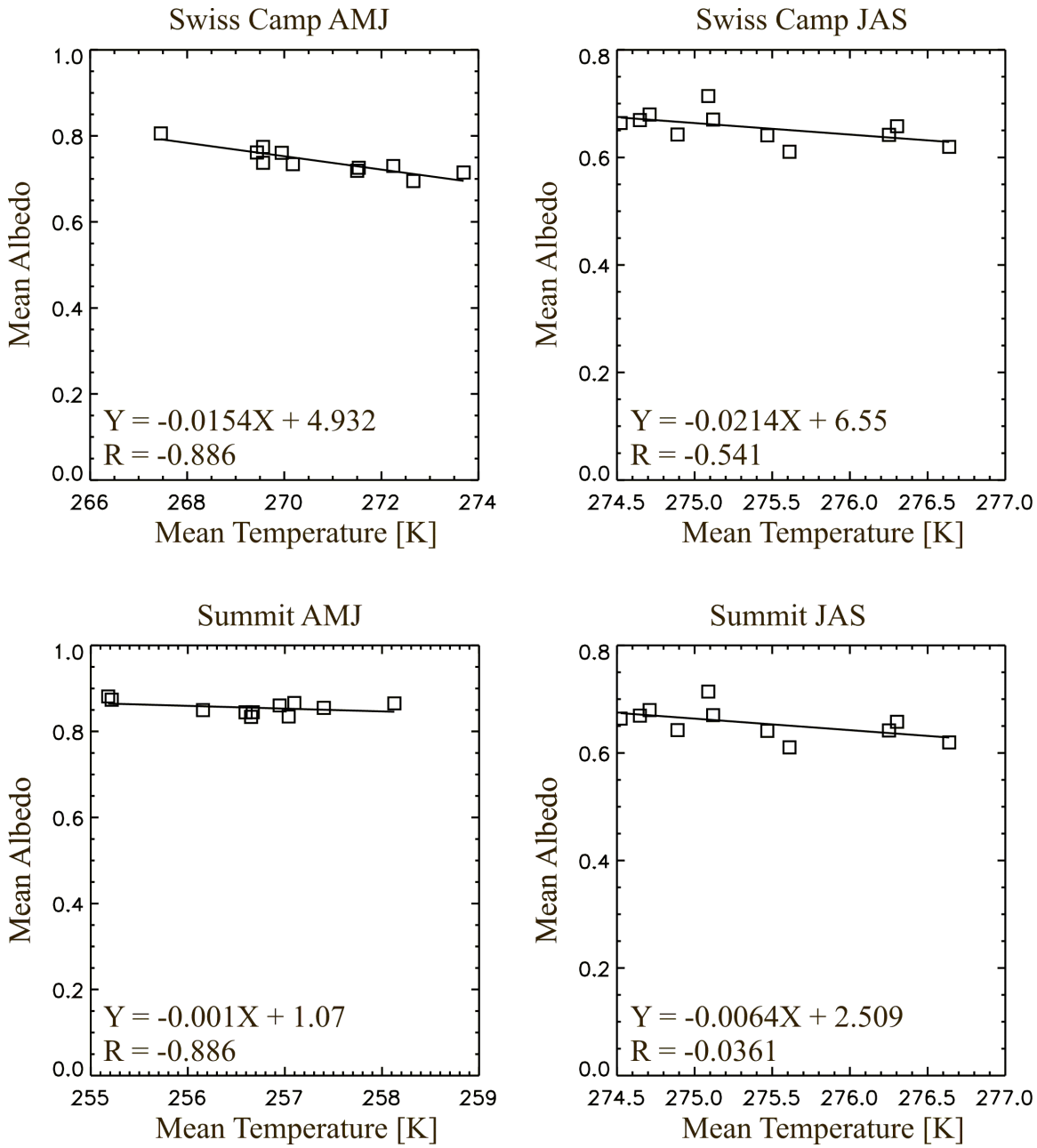

Figure 4.8a Correlation between seasonal mean albedo and temperature at GC-Net weather stations. AMJ refers to the April-May-June period. JAS refers to the July-August-September period.

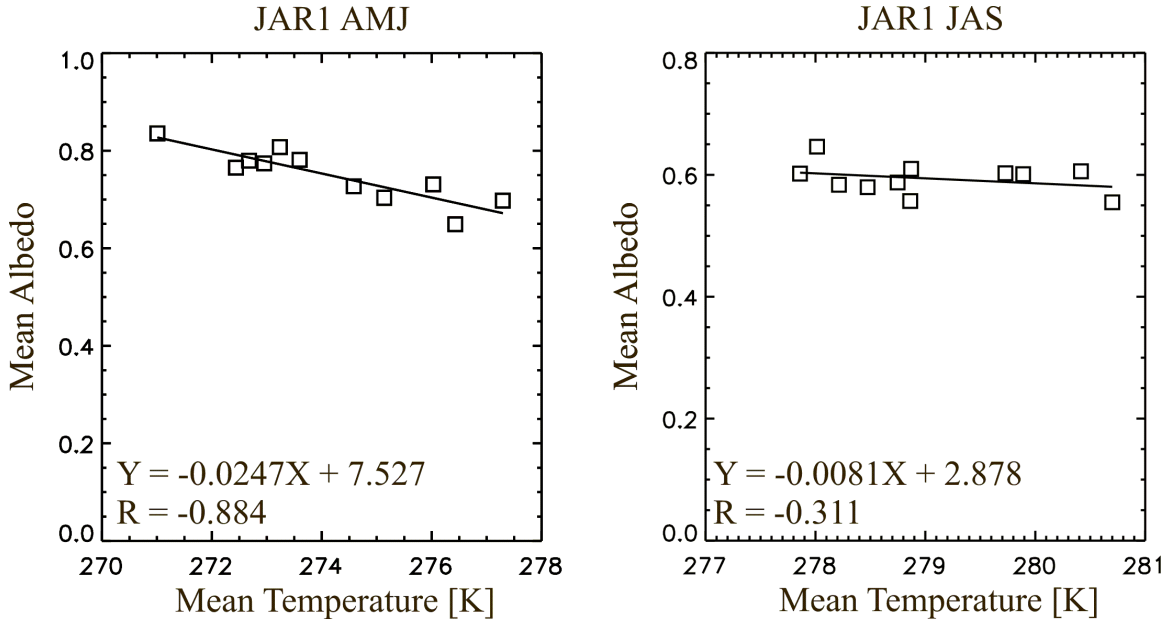

Figure 4.8b Same as **Figure 4.8a**

e. Sensitivity Study

A sensitivity study is conducted to quantify the albedo trend impact on solar radiation absorption and melt-water production (**Table 4.2**). Mean downward solar irradiance is calculated from Polar MM5 output and multiplied by the albedo reduction to determine change in solar energy reflection/absorption. Areas with albedo lower than 0.70 are assumed to be melting, allowing the determination of ice to water conversion potential. Results for the early melt period demonstrate total additional solar energy absorption of 48.0 eJ and 96.6 eJ for AVHRR and MODIS, respectively, representing sufficient energy to generate 1.7 km^3 and 3.1 km^3 of melt water. The late melt season solar energy changes are larger, that is, 346.0 eJ and 1330.0 eJ of absorbed solar energy, corresponding to 11.1 km^3 and 42.6 km^3 of melt water if all extra energy is used for melting. To give some perspective, according to the U.S. Department of Energy, the 2005 total U.S. electricity production was 1.45 eJ.

Table 4.2 Results from albedo-melt energy study

Parameter	AVHRR (1982-1999)		MODIS (2000-2005)	
	Early to Mid Melt	Mid to Late Melt	Early to Mid Melt	Mid to Late Melt
Albedo Trend*	-0.006	-0.008	-0.006	-0.008
Additional Solar Energy Absorption (eJ)	48.9	346.0	96.6	1330.0
Additional Melt-water Volume (km^3)	1.7	11.1	3.1	42.6

*Mean trend for entire ice sheet.

f. Melt Area

Seasonal mean albedo data are used to determine melt extent trends. In this study, pixels with a mean albedo less than 0.7 are defined as melting. The time series of melt extent is examined for the early to mid, mid to late, and entire melt season (**Figure 4.9**). Positive melt extent trends occur in all time periods. The largest trend occurs during the early melt season with a melt extent increase of 18,663 $km^2\ y^{-1}$. The trend for the entire melt season is 3,020 $km^2\ y^{-1}$, corresponding to an annual increase of ~0.2% y^{-1}. Abdalati et al. (2000) found the melt extent trend to be ~1.0% y^{-1}; however they investigated trends in maximum melt extent. Furthermore, microwave techniques are probably more sensitive to surface melting than reflectance in the visible and near infrared portion of the electromagnetic spectrum (Zwally, 1977),

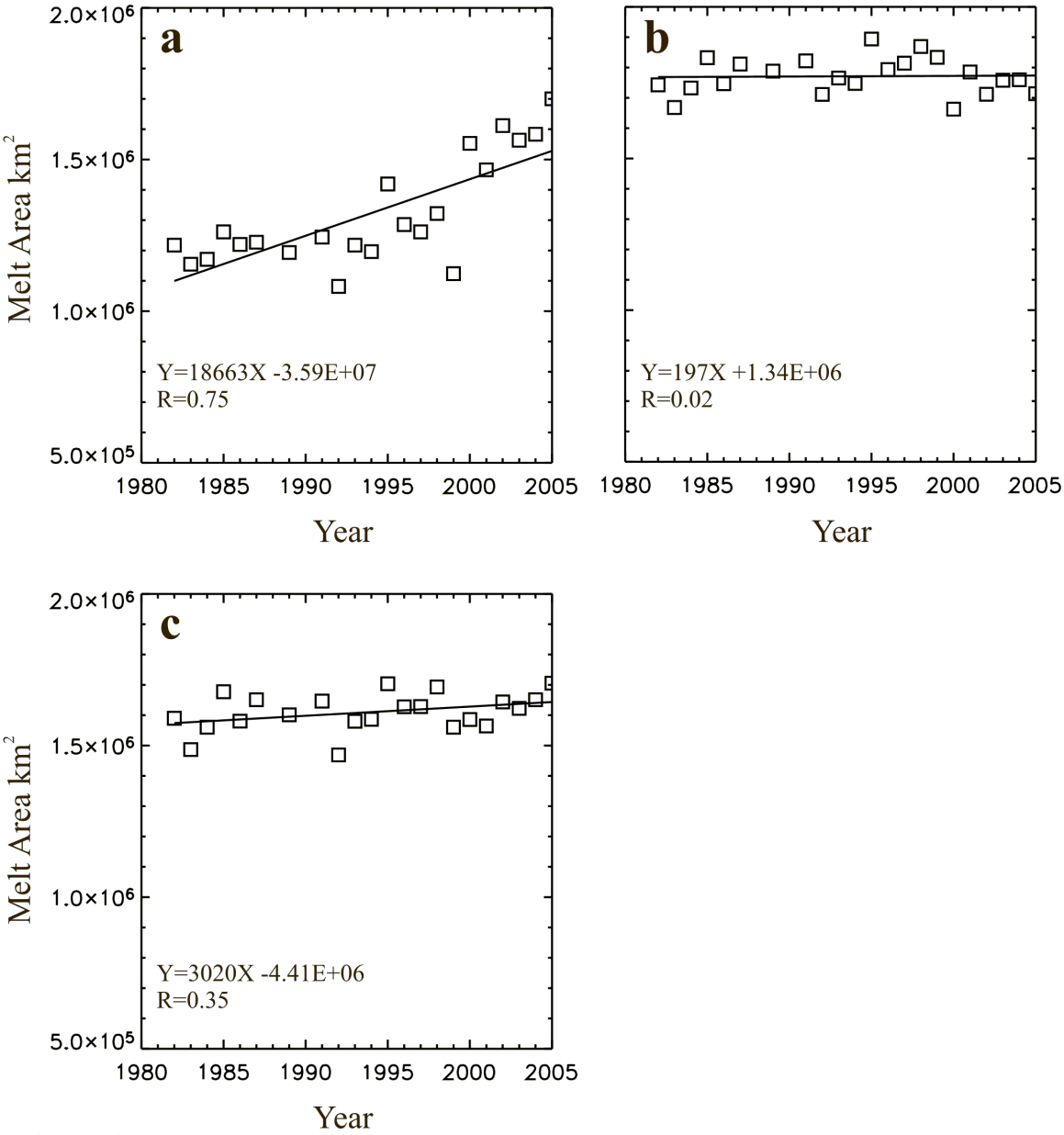

Figure 4.9 Changes in Greenland ice sheet melt area for the period 1982-2005 using an albedo threshold of 0.7. a.) Early melt. b.) Late melt. c.) Entire melt season.

6 Conclusions

In this study, albedo data from space-borne sensors AVHRR and MODIS were used to assess Greenland ice sheet albedo changes over the 1982-2005 period. Sensor bias and errors were evaluated using *in-situ* albedo observations from GC-Net AWS. Negative albedo biases were evident in AVHRR and MODIS data. Biases, even if not completely corrected, do not substantially affect the results of this study, since the goal of this study is a trend analysis. Trend analysis was performed separately for AVHRR and MODIS, as data temporal in-homogeneity could not be completely resolved. Nonetheless, significant albedo reductions are evident along ice sheet margins and the southern ice sheet in both AVHRR and MODIS periods. Negative albedo trends increase solar energy absorption and promote enhanced melt water production. Observations of increased melt extent are consistent with trends detected by an independent microwave remote study (Abdalati et al., 2000).

Temperature, grain size, and the presence of impurities are the primary determinants of snow albedo, thus albedo trends are a function of these three variables. An albedo-temperature correlation study demonstrates that temperature increases at least partly explain negative albedo trends. Temperature explains at least two thirds of the variance in ice sheet margin albedo and correlation is commonly statistically significant at or above the 95% confidence level.

Albedo-temperature correlations are higher during the early melt season than in the late melt season. Thus, early melt season temperatures are arguably more important in determining ice sheet sensitivity to albedo induced climate change. Late melt season albedo is not as strongly correlated with temperature due impart to decreased temperature

variability, resulting from latent energy sinks (i.e. melt and evaporation). The greatest change in melt extent also occurs during the early melt season. Thus, early season temperatures appear critically important in determining melt rates.

AVHRR bias assessment is hindered by the use of 24km data and surface in-homogeneity issues. For example, at the JAR1 and JAR2 where surface melting and patchiness is largest, variable surface conditions confound bias assessment.

Uncertainty in trend analysis arises from several sources. Cloud detection over snow and ice surfaces remains a challenge as surface and cloud radiation properties are so similar. Incorrectly labeling a cloudy pixel as clear could produce either anonymously high or low albedo values depending on surface albedo and cloud properties. The use of seasonal mean albedo in trend analysis minimizes cloud detection errors. Geo-location errors are another source of AVHRR uncertainty. AVHRR geo-location errors are typically 2-3 km; however the error can be as a large as 10-12 km. Additional uncertainty results from IDEA albedo retrieval at solar zenith angles near 75° as algorithm errors increase with increasing solar zenith angle.

Several steps could be taken to improve the methodology of this study. Cloud detection could be improved through by using manual cloud masking in place of a simple single channel threshold. Albedo trend analysis could be performed using higher resolution data, as 5 km AVHRR and 0.5 km MODIS albedo data are available. Higher resolution AVHRR data would also benefit sensor bias calculations and dataset inter-calibration. Future work could focus on improved cloud detection and exploration of additional remote sensing applications using MODIS.

5 Acknowledgements

This work was supported by NASA grant NNG04GH70G and an Ohio State University Honor's Scholarship. Special gratitude is due to my advisor, Dr. Jason Box for extensive guidance, input, and editing. Thanks go to Dr. Shunlin Liang for providing the Improved Direct Estimate Algorithm; Dr. Jeff Key for providing the APPx dataset; Dr. Julienne Stroeve for providing a previous basis for this study; and Dr. David Bromwich for providing Polar MM5 data.

6 References

Abdalati, W., K. Steffen, 2001: Greenland ice sheet melt extent, *J. Geophys. Res.*, **106**, 33,983-33,988

Baldwin, D. and W.J. Emery, 1995: Spacecraft attitude variations of NOAA-11 inferred from AVHRR imagery. Int. *J. Rem. Sen*, **16**, 531-548.

Bohren, C.F., and B.R. Barkstrom, 1974: Theory of the optical properties of snow. *J. Geophys. Res*., **79**, 4,527-4,535.

Box, J. E., D. H. Bromwich, and L-S. Bai, 2004: Greenland ice sheet surface mass balance 1991–2000: Application of Polar MM5 mesoscale model and in situ data, *J. Geophys. Res.*, **109**, D16105, doi:10.1029/2003JD004451.

Box J. E., and A. Rinke, 2003: Evaluation of Greenland Ice Sheet Surface Climate in the HIRHAM Regional Climate Model Using Automatic Weather Station Data. *J. Climate,* **16**, 1,302-1,319.

Box, J. E., 2002: Survey of Greenland instrumental temperature records: 1873–2001. *Int. J. Climatol*., **22**, 1,829-1,847.

Bromwich, D.H., L-S. Bai, and G.G. Bjarnason, 2005: High Resolution Regional Climate Simulations over Iceland Using Polar MM5. *Mon. Wea. Rev.,* **133**, 3,527-3,547.

Cappelen J., 2004: Yearly mean temperature for selected meteorological stations in Denmark, the Faroe Islands and Greenland, 1873-2003. Tech. Rep. 04-07, 9 pp, Danish Meteorological Institute, Copenhagen.

Clark P., N.G. Pisias, T.F. Stocker, and A.J. Weaver, 2002: The role of the thermohaline circulation in abrupt climate change. *Nature,* **415**, 863-869.

Clarke, A.D: and K.J. Noone, 1985: Soot in the Arctic Snowpack: A Cause for Perturbations in Radiative Transfer. *Atmo. Enviro.*, **19**(12), 2,045-2,053.

Church, J. A., J. M. Gregory, P. Huybrechts, M. Kuhn, C. Lambeck, M. T. Nhuan, D.Qin, and P. L. Woodworth, 2001: Changes in sea level, in Climate Change 2001: The Scientific Basis, edited by J. T. Houghton et al., 639– 694, Cambridge Univ. Press, New York.

Cuffey, K. M., and M. K. Yau, 2000: Substantial contribution to sea-level rise during the last interglacial from the Greenland ice sheet. *Nature*, **404**, 591-594.

Grenfell, T.C., B. Light, and M. Sturm, 2002: Spatial distribution and radiative effects of soot in the snow and sea ice during the SHEBA experiment. *J. Geophys. Res.,* **107**(C10), doi:10.1029/2000JC000414.

Greuell, W., and W.H. Knap, 2000: Remote sensing of the albedo and detection of the slush line on the Greenland ice sheet. *J. Geophys. Res*., **105** (D12), 15,567-15,576.

Greuell, W., C.H. Reimer, and J. Oerlemans, 2002: Narrowband-to broadband albedo conversion for glacier ice and snow based on aircraft and near-surface measurements. *Rem Sen Enviro*, **82**, 48-63.

Hansen J. and L. Nazarenko, 2003: Soot Climate forcing via snow and ice albedos. *Proc. Natl. Acad. Sci.* **101**, 423-428, doi:10.1073/pnas.2237157100.

Haran T., 2001: The MODIS Swath to Grid Toolbox. University of Colorado, Boulder, CO 80309-0449, http://gcmd.nasa.gov/records/MS2GT.html

Holland, M.M., Schramm, J.L., and J.A. Curry, 1997: Thermodynamic feedback processes in a single-column sea-ice-ocean model, *Annals of Glaciology*, **25**, 327-332.

Key J., C. Fowler, J. Maslanik, T. Haran, T. Scambos, and W. Emery, 2002: The Extended AVHRR Polar Pathfinder (APP-x) Product, v 1.0. Digital Media, Space Science and Engineering Center, University of Wisconsin, Madison, WI.

Konzelmann, T. and A. Ohmura, 1995: Radiative fluxes and their impact on the energy balance of the Greenland ice sheet, *J. Glaciol.,* **41**(139), 490-502.

Laine, V., 2004: Artic sea ice regional albedo variability and trends, 1982-1998. *J. Geophys. Res.,* **109**, C06027, doi:10.1029/2003JC001818.

Liang, S, 2001: Narrow to Broadband Conversion of Land Surface Albedo I Algorithms. *Rem Sen Envirot*, **76,** 213-238.

Liang, S., J. Stroeve, J., J. E. Box, 2005: Mapping daily snow shortwave broadband albedo from MODIS: the improved direct estimation algorithm and validation. *J. Geophys. Res.*, **110,** D10109.

Lüthje M., L. T. Pedersen, N. Reeh, W. Greuell, 2006: Modelling the evolution of supraglacial lakes on the West Greenland ice-sheet margin, *J. Glaciol*., accepted

Ohmura, A., P. Calanca, M. Wild, and M. Anklin, 1999: Precipitation, accumulation, and mass balance of the Greenland ice sheet. *Zeit. Gletsch. Glazialgeol*, **35**, 1-20.

Rao, C. R. N. and J. Chen, 1995: Inter-satellite calibration linkages for the visible channels of the Advanced Very High Resolution Radiometer on the NOAA-8, -9, and –11. *Int. J. Rem. Sen.,* **16**, 1,931-1,942.

Rigor, I., R. Colony, and S. Martin, 2000: Variations in Surface Air Temperature Observations in the Arctic, 1979 - 1997, *J. Climate*, **13**(5), 896-914.

Schaaf, C. B., F. Gao, A. H. Strahler, W. Lucht, X. Li, T. Tsang, N. C. Strugnell, X. Zhang, Y. Jin, J.-P. Muller, P. Lewis, M. Barnsley, P. Hobson, M. Disney, G. Roberts, M. Dunderdale, C. Doll, R. d'Entremont, B. Hu, S. Liang, and J. L. Privette, 2002: First standard BRDF, albedo and nadir reflectance products from MODIS. *Rem. Sen. Enviro.*, **83**, 135-148.

Steffen, K. and J.E. Box, 2001: Surface climatology of the Greenland ice sheet: Greenland Climate Network 1995-1999. *J. Geophys. Res.*, **106**(D24), 33,951-33,964.

Steffen, K., J. E. Box, and W. Abdalati, 1996: Greenland Climate Network: GC-Net. US Army Cold Regions Reattach and Engineering (CRREL), CRREL monograph, tribute to M. Meier.

Stroeve, J., 2001: Assessment of Greenland albedo variability from the advanced very high resolution radiometer Polar Pathfinder data set. *J. Geophys. Res.,* **106**(D24), 33,989-34,006.

Stroeve, J, J. E. Box, A. Nolin, S. Liang, C. Schaaf, F. Gao, 2005: Accuracy assessment of the MODIS 16-day albedo product for Snow: comparisons with Greenland in situ measurements. *Remote Sensing of the Environment*, **94**(1), 46-60.

Trepte et al., 2001: Development of a daytime polar cloud-mask using theoretical models of near-infrared bidirectional reflectance for ARM and CERES. NASA Langley Cloud and Radiation Minnis Group. http://www-pm.larc.nasa.gov/data/fire3/publications/Trepte.polar.abs.pdf

van den Broeke, M., D. van As, C. Reijmer, R. van de Wal, 2004: Assessing and improving the quality of unattended radiation observations in Antarctica. *J. Atmos. and Ocean. Tech*, **21**(9), 1,417-1,431.

van der Veen, C. J., 2002: Polar ice sheets and global sea level: how well can we predict the future?. *Glob. Plan. Chng*., **32**, 165-194.

Warren, S.G., 1982: Optical properties of snow. *Rev. Geophys. Space Phys*., **20**, 67-89.

Warren, S.G., 1984: Impurities in snow: effects on albedo and snowmelt. *Ann. Glaciol*., **5**, 177-179.

Wiscombe, W.J., and S.G. Warren, 1980: A model for the spectral albedo of snow, I: *Pure snow. J. Atmos. Sci.,* **37**, 2712-2733.

Zwally, H.J., 1977: Microwave emissivity and accumulation rate of polar firn. *J. Glaciol*., **18**, 195–216.

Zwally, H. J., and M. B. Giovinetto, 2000: Spatial distribution of surface mass balance on Greenland, *Ann. Glaciol.*, **31**, 126–132.

Zwally et al., 2002: Surface Melt-Induced Acceleration of Greenland Ice-Sheet Flow, *Science,* **297**, 218-222.